# Role of the Bifunctional Aminoacyl-tRNA Synthetase EPRS in Human Disease

Honors Research Thesis

Presented in partial fulfillment of the requirements for graduation *with honors research distinction* in Biochemistry in the undergraduate colleges of The Ohio State University

by
Nathan Kudlapur

The Ohio State University
April 2020

Project Advisor: Dr. Karin Musier-Forsyth, Department of Chemistry & Biochemistry

# Table of Contents

## Acknowledgements

First, I would like to thank my research advisor, Dr. Karin Musier-Forsyth, for supporting me and my research efforts over the past several years. I have learned so much during my time in your lab—about research, about biochemistry, and about life. Thank you for mentoring me, encouraging me, and helping me get to where I am today.

I would like to thank all the members of the Musier-Forsyth lab for their support, encouragement, advice, and friendship. I am extremely grateful to be a part of the KMF group with all of you. I would also like to thank all of my professors, friends, and family for supporting and encouraging me throughout my research endeavors at Ohio State.

I am grateful to the College of Arts & Sciences and the Office of Undergraduate Research & Creative Inquiry for providing funding for my project.

Finally, I would like to thank my graduate student mentor, Danni Jin. I would not be where I am today without you. Thank you for your mentorship, guidance, and support. Thank you for answering my frequent questions and reviewing my many drafts of proposals, abstracts, posters, and presentations. You're the best.

## Abbreviations

| | |
|---|---|
| AARS | Aminoacyl-tRNA synthetase |
| ATP | Adenosine triphosphate |
| eIF2α | Eukaryotic translation initiation factor 2 alpha |
| EPRS | Glutamyl-prolyl-tRNA synthetase |
| ERS | Glutamyl-tRNA synthetase |
| FA | Fluorescence anisotropy |
| GST | Glutathione *S*-transferase |
| ISR | Integrated stress response |
| MALS | Multi-angle light scattering |
| MBP | Maltose-binding protein |
| MSC | Multi-aminoacyl-tRNA synthetase complex |
| mTOR | Mammalian target of rapamycin |
| PAGE | Polyacrylamide gel electrophoresis |
| $PP_i$ | Pyrophosphate |
| PRS | Prolyl-tRNA synthetase |
| RC | Random coil |
| SEC | Size exclusion chromatography |
| SLIM | Site-directed, ligase-independent mutagenesis |
| SUMO | Small ubiquitin-like modifier |
| WT | Wild-type |

## Abstract

Aminoacyl-tRNA synthetases (AARS) are a class of enzymes that catalyze the charging of tRNAs with cognate amino acids, a critical step that contributes to the fidelity of protein synthesis. Many AARSs also possess noncanonical functions such as regulation of apoptosis, mRNA translation, and RNA splicing. Some AARSs have evolved new domains with no apparent connection to their charging functions. For example, WHEP domains were originally identified in tryptophanyl-tRNA synthetase (WRS), histidyl-tRNA synthetase (HRS), and glutamyl-prolyl-tRNA synthetase (EPRS). EPRS is a unique bifunctional AARS, found only in higher eukaryotes, and consists of glutamyl-tRNA synthetase (ERS) and prolyl-tRNA synthetase (PRS) joined by a non-catalytic linker containing three WHEP domains in humans. Two compound heterozygous point mutations within human ERS (P14R and E205G) have been identified in the genomes of two patients with type 1 diabetes and bone disease. However, the mechanism by which these mutations contribute to disease is unknown. Our goal is to determine whether the point mutations affect the canonical catalytic activity of EPRS responsible for tRNA charging or noncanonical functions. Both P14 and E205 are highly conserved residues located in the GST and catalytic domain, respectively. An ERS variant appended to 2.5 WHEP domains ($ERS_{2.5W}$) has been purified and shown to display robust tRNA binding and aminoacylation activity *in vitro*. The P14R and E205G single mutants display the same binding affinity for $tRNA^{Glu}$ as WT $ERS_{2.5W}$, suggesting that the observed defect is at the catalytic step. Whereas the $ERS_{2.5W}$ P14R mutant has near wild-type (WT) aminoacylation activity, the $ERS_{2.5W}$ E205G variant has a severe aminoacylation defect. Both mutations, however, lead to reduced amino acid activation. Together with a collaborator, we are currently characterizing the effect of these two mutations on cell proliferation and the integrated stress response. Taken together, this work has important implications for the understanding of AARS-related human disease mechanisms and development of new therapeutics.

## Introduction

Aminoacyl-tRNA synthetases (AARS) are an ancient class of enzymes that catalyze the aminoacylation, or "charging," of a tRNA with its cognate amino acid, a critical step that contributes to the fidelity of protein synthesis (Ibba & Söll, 2000). The reaction catalyzed by AARSs includes two steps: (1) activation of an amino acid and formation of the aminoacyl adenylate intermediate (AA-AMP), and (2) transfer of the amino acid from AA-AMP to the 3′ end of a cognate tRNA. This two-step reaction is illustrated in Figure 1.

$$AA + ATP \leftrightarrow AA\text{-}AMP + PP_i$$

$$AA\text{-}AMP + tRNA \rightarrow AA\text{-}tRNA + AMP$$

**Figure 1**. Aminoacylation occurs as a 2-step reaction: activation of amino acid with ATP, and transferring of amino acid to tRNA

By pairing amino acids with specific anticodon sequences on tRNAs, AARSs are pivotal in the physical interpretation of the genetic code. This crucial function of AARSs is evidenced by their ubiquity, as they are present in cells from all three domains of life—archaea, bacteria, and eukarya (Woese et al., 2000).

As 20 proteogenic amino acids exist within the cell, organisms possess 20 different AARSs, although some exceptions exist. For example, some species of archaea and bacteria have been found with as few as 16 AARSs (Bult et al., 1996; Smith et al., 1997). One strategy that species lacking a full complement of AARS employ to enable proper translation is the use of tRNA-dependent amino acid transformation pathways, such as forming Gln-$tRNA^{Gln}$ from Glu-$tRNA^{Gln}$ (Ibba et al., 2000).[1]

[1] AARSs are denoted either by the three letter amino acid abbreviation followed by "RS," or by the single letter amino acid abbreviation followed by "RS."

AARSs are separated into two classes based on structural and chemical differences. Class I AARSs contain a Rossman fold within the catalytic active site and aminoacylate at the 2′ OH. Class II AARSs contain an antiparallel β-fold in the active site and aminoacylate at the 3′ OH (Eriani et al., 1990). In addition, class I AARSs bind ATP in a straight conformation and approach tRNA from the minor groove side, while class II AARSs bind ATP in a bent conformation and approach tRNA from the major groove side (Arnez & Moras, 1997). Finally, class I AARSs primarily function as monomers, while class II AARSs function as multimers (Bullwinkle & Ibba, 2014). All AARSs contain a catalytic domain and an anticodon binding domain.

In eukaryotic systems a number of AARSs possess noncanonical functions in addition to tRNA charging. These include a host of activities completely unrelated to aminoacylation, such as regulation of apoptosis, signal transduction, and RNA splicing (reviewed in Yao & Fox, 2013). For example, a proteolysis fragment of TyrRS plays a role in inducing angiogenesis (Wakasugi et al., 2002), LeuRS plays a role in tumorigenesis by interacting with the RagD GTPase to stimulate the mammalian target of rapamycin (mTOR) pathway (Han et al., 2012), and MetRS plays a role in rRNA synthesis through translocation to the nucleus in response to cellular growth signals (Ko et al., 2000).

In higher eukaryotes, a subset of AARSs assemble to form the multi-aminoacyl-tRNA synthetase complex (MSC) (Kisselev & Wolfson, 1994). Primitive forms of the MSC have been described in archaea (Praetorius-Ibba et al., 2007; Raina et al., 2012), but these complexes do not possess any auxiliary proteins. Throughout evolution in eukaryotes, the MSC grew increasingly more complex, incorporating accessory proteins that facilitate MSC assembly (Havrylenko & Mirande, 2015). The emergence of the MSC throughout evolution is summarized in Figure 2.

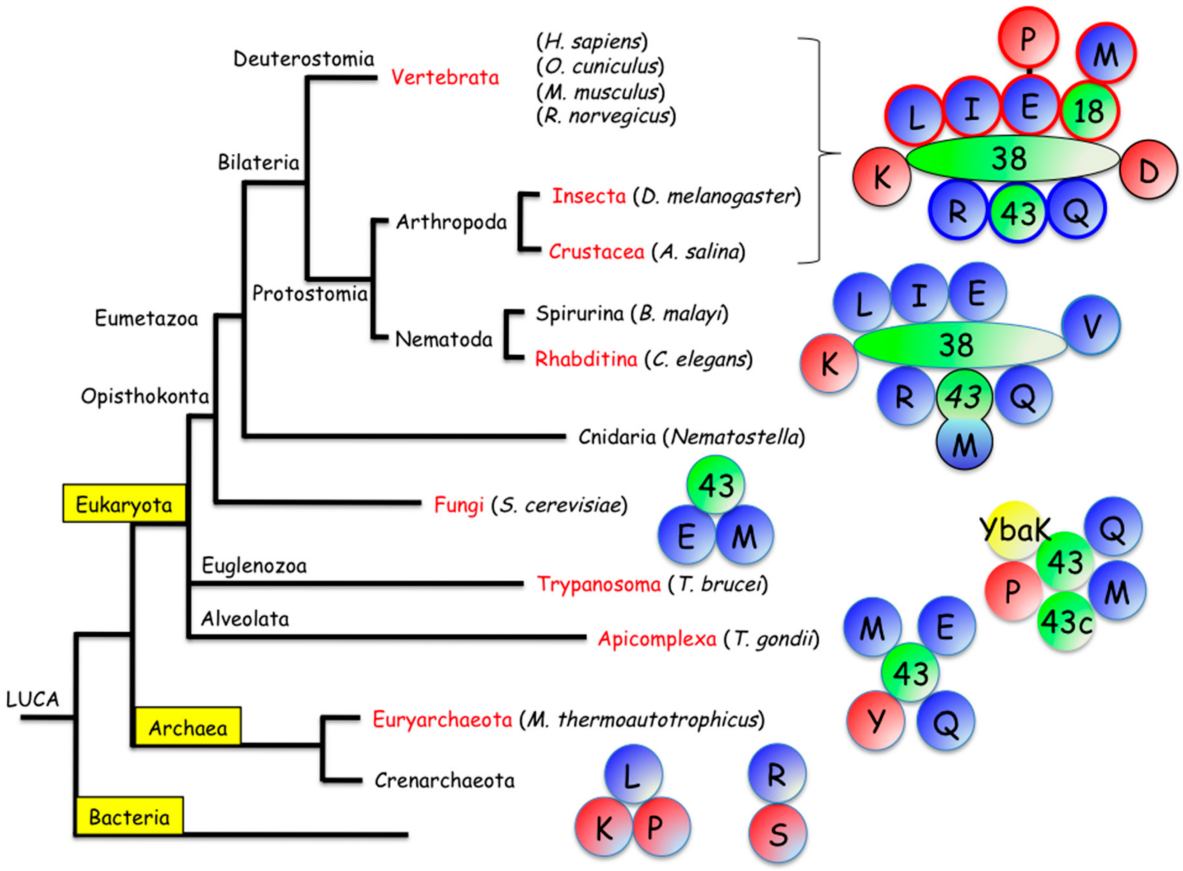


**Figure 2.** Emergence of the multi-aminoacyl-tRNA synthetase complex (MSC) throughout evolution (Havrylenko & Mirande, 2015). The auxiliary proteins which play a structural role in the MSC are shown in green. Class I AARSs are shown in blue; class II in red. AARSs are denoted in this figure by the one letter symbol of their amino acid substrate. YbaK, shown in yellow, is an autonomous editing protein. The MSC grew increasingly more complex throughout evolution in eukaryotes, acquiring auxiliary scaffold proteins. Archaeal forms of the MSC possess distinct differences, however, and suggest a separate origin.

Although a primitive form of the MSC exists in archaea, distinct differences from eukaryotic MSCs suggest a separate origin (Laporte et al., 2014). First, in terms of the mode of assembly, eukaryotic MSCs always assemble through protein-protein interaction domains found on auxiliary scaffold proteins. Versions of these scaffold proteins in lower eukaryotes are structural homologs of the metazoan scaffold proteins, which supports conservation of the MSC in eukarya. In archaea, however, assembly is mediated by AARSs themselves. Second, archaeal MSCs consist primarily

of class II AARSs, whereas eukaryotic MSCs are most abundant in class I AARSs. Class I and class II AARSs are themselves evolutionarily distinct, and taking all of these observations together suggests that archaeal and eukaryotic MSCs arise from separate origins.

In humans, the MSC consists of nine different AARS activities in eight proteins— IleRS, LeuRS, MetRS, GlnRS, LysRS, ArgRS, AspRS, and Glu-ProRS—along with three non-enzymatic scaffold proteins, AARS-interacting multifunctional proteins (AIMPs) (Robinson et al., 2000). The current working model of the MSC is shown in Figure 3.

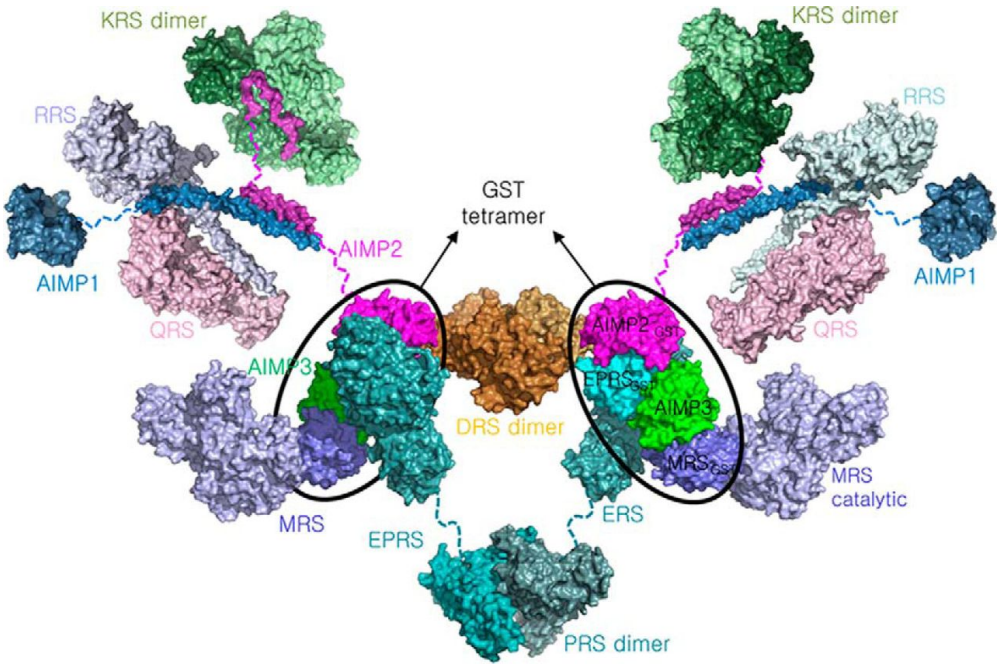


**Figure 3.** Proposed structure for the MSC (Cho et al., 2015). The MSC is thought to have an overall dimeric structure formed by DRS and PRS dimers. In addition, a gluthione *S*-transferase (GST) tetramer formed by four different MSC components serves as an important platform for MSC assembly.

AIMP1-3 play a crucial role in maintaining structural integrity of the MSC. For example, depletion of AIMP2 triggers a massive disintegration of the MSC (Kim et al., 2002). The MSC is proposed to have an overall dimeric structure, joined by aspartyl-tRNA synthetase (DRS) and prolyl-tRNA synthetase (PRS) dimers. In addition, glutathione *S*-transferase (GST) domains shared by AIMP2,

AIMP3, glutamyl-tRNA synthetase (ERS), and methionyl-tRNA synthetase (MRS), form a heterotetramer that serves as a unique and dynamic platform for MSC assembly (Cho et al., 2015).

Although the complete function of the mammalian MSC remains unclear, it is thought to facilitate substrate channeling and translation as well as controlling the cellular turnover of AARSs (Lee et al., 2004). In addition, the MSC serves as a hub for many noncanonical AARS functions. While AARSs are usually localized in the MSC for tRNA charging, components of the MSC may be inducibly released from the complex to participate in a variety of functions elsewhere in the cell (Kim et al., 2014).

Mutations in AARSs have been linked to a number of diseases, including neuronal diseases, cancer, metabolic disorders, and autoimmune disorders (Yao & Fox, 2013; Park et al., 2008). The diverse connection of AARSs to disease can be seen in the linkage map in Figure 4. Of note, these disease-related AARSs include both MSC-component AARSs and free AARSs. The connection of AARSs to disease may be related to either their tRNA charging or noncanonical function. For example, diminished aminoacylation activity of LysRS has been linked to Charcot-Marie-Tooth (CMT) disease, a neurological disorder (McLaughlin et al., 2010). However, the catalytic activity is normal in mutated versions of TyrRS linked to CMT disease, which suggests a noncanonical mechanism (Froelich & First, 2011). With the various pattern of enzymatic activity of mutated AARSs in disease, the involvement of AARSs in disease pathologies is increasingly gaining attention.

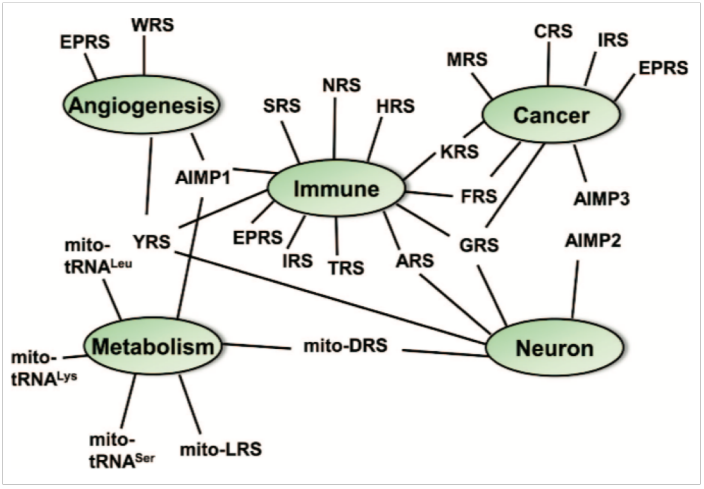


**Figure 4.** Linkage map of AARSs with various human diseases (Park et al., 2008).

Some AARSs have evolved new domains with no apparent connection to their charging functions. These include a specialized amino-terminal helix (N-helix), GST domain, leucine zipper (LZ) motif, endothelial monocyte-activating polypeptide II (EMAP II) domain, and WHEP domains (Guo, Yang, & Schimmel, 2010). Given the lack of function of these domains in tRNA charging, it is likely that they play a role in noncanonical functions. In particular, they serve important roles in MSC assembly (Cho et al., 2015). WHEP domains were originally identified in tryptophanyl-tRNA synthetase (WRS), histidyl-tRNA synthetase (HRS), and glutamyl-prolyl-tRNA synthetase (EPRS). The latter enzyme is a unique example of a bifunctional AARS, found only in higher eukaryotic systems, that consists of two synthetase domains—ERS and PRS—joined by a non-catalytic linker region containing WHEP domains. Given the unique bifunctional nature of EPRS, it serves as an intriguing enzyme to study.

Our collaborators, Dr. Ron Wek (Indiana University School of Medicine) and Dr. Orly Elpeleg (Hadassah Medical Center, Israel), have identified two compound heterozygous point mutations—P14R and E205G[2]—within the ERS portion of the human EPRS genes of two Ashkenazi Jewish patients with type 1 diabetes and bone disease. However, the mechanism by which these mutations contribute to disease is unknown. In this thesis, I will investigate these point mutations in EPRS to determine whether they affect the canonical activity of EPRS responsible for tRNA charging or noncanonical functions. This work will enhance our understanding of AARS-related human disease mechanisms and may contribute to the development of new therapeutics.

[2] This nomenclature for point mutations indicates the original amino acid, the position of mutation, and the new amino acid after mutation. Thus, P14R indicates that a proline at residue 14 is mutated to arginine, and E205G indicates that a glutamate at residue 205 is mutated to glycine.

# Chapter 1: Purification of Human Glutamyl-tRNA Synthetase

## Introduction

Human EPRS is a 172 kDa protein that contains four domains: an N-terminal GST domain, two catalytic domains (ERS and PRS), and a linker domain containing three tandem WHEP domains (Jia et al., 2008) (see Figure 5). Each WHEP domain is 50 amino acids long and possesses a helix-turn-helix structure (Cahuzac et al., 2000). GST domains are found in a number of different AARSs and other translational factors (Koonin et al., 1994; Guo & Yang, 2014), and they are thought to play a role in protein assembly and folding (Cho et al., 2015). ERS is a class I AARS, while PRS is a class II AARS.

Numerous noncanonical functions of EPRS are known. Phosphorylation at specific serine residues within the linker promote participation of EPRS in the GAIT (interferon-γ-activated inhibitor of translation) system, leading to silencing of inflammation-related mRNAs (Arif et al., 2009). Another site-specific phosphorylation in the linker directs antiviral immune response during infection of RNA viruses (Lee et al., 2016). EPRS also facilitates long chain fatty acid uptake in insulin-treated adipocytes (Arif & Fox, 2017). Critical to all of these noncanonical functions is the release of EPRS from the MSC via linker phosphorylation.

Full-length human EPRS has never before been purified. Previous attempts have encountered either poor expression or solubility (Lei et al., 2015). However, individual components ERS and PRS have been purified. Though purified PRS displayed robust aminoacylation activity, purified ERS displayed very weak catalytic activity (Halawani et al., 2018). To lay the groundwork for studying the ERS point mutations P14R and E205G, we first sought to purify an active wild-type (WT) ERS construct.

## Materials and Methods

### *Plasmid Construction*

The plasmid encoding human EPRS was a gift from Dr. Paul Fox (Cleveland Clinic). The backbone vector, SUMO pRSF MBP, was a gift from Dr. Kotaro Nakanishi (Ohio State). Three ERS genes, ERS (aa. 1-687), $ERS_{RC}$ (aa.1-749), and $ERS_{2.5W}$ (aa.1-929), were cloned into the SUMO pRSF MBP vector between SalI and NotI restriction sites. Cloning was confirmed by Sanger sequencing.

### *Protein Preparation*

All three human ERS variants were purified using the same procedure. *Escherichia coli* BL21(DE3)RIL was transformed with the ERS-encoding plasmid and protein expression was induced with 0.1 mM isopropyl β-D-thiogalactopyranoside (IPTG) at 16 °C overnight. Cells were harvested by centrifugation and resuspended in lysis buffer (8 mL / g cell pellet) (500 mM NaCl, 25 mM Tris-HCl pH 8, 5 mM imidazole, 5% glycerol, 3 mM 2-mercaptoethanol, and protease inhibitor). Cells were lysed by incubation with 10 mg/mL lysozyme on ice for 30 min and moderate sonication. To remove nucleic acid, cell lysate was incubated with 0.5% v/v polyethyleneimine (PEI) on ice for 30 min. Precipitated nucleic acid and cell debris were removed by centrifugation for 30 min at 15,000 g at 4 °C. Proteins were precipitated with 375 mg/mL ammonium sulfate, resuspended in 20 mL lysis buffer, and then filtered through a 0.45 μm syringe filter. The filtered cell lysate was loaded onto a nickel (II) column, equilibrated with lysis buffer. The column was washed with lysis buffer, and the protein was then eluted with buffers containing 10-100 mM imidazole. Elution fractions containing ERS—as confirmed by SDS-PAGE analysis—were pooled and dialyzed with SUMO protease overnight. The digested protein was concentrated and further

purified using size-exclusion chromatography (SEC) on a Superdex 200 16/60 column. Proteins were stored at -20 °C at approximately 100 μM in 40% glycerol.

*Size-exclusion chromatography / multi-angle light scattering (SEC/MALS)*

Protein samples were run on the Akta Pure 25M (GE) coupled to a Dawn Helios 8+ (Wyatt) multi-angle light scattering system equipped with an Optilab TrEX refractive index detector and Wyatt QELS quasi-elastic light scattering detector (Wyatt). Approximately 100 μg protein in 500 μL total volume was separated over a Superose 6 Increase column (GE) at 0.4 mL/min. Molecular weights were calculated using Astra 7 software.

*RNA Preparation*

The transcription template for human $tRNA^{Glu\ (TTC)}$ was prepared from a pIDTsmart plasmid through digestion with FokI restriction endonuclease. The tRNA was prepared via *in vitro* transcription with T7 RNA polymerase using a standard protocol (Milligan & Uhlenbeck, 1989) and run on a 12% urea-PAGE gel. The desired band was excised, crushed, and soaked in RNA elution buffer (0.5 mM $NH_4OAc$, 1 mM EDTA) overnight at 37°C with shaking at 200 rpm. The RNA was then isolated through butanol extraction of the supernatant and subsequent ethanol precipitation.

*Aminoacylation Assays*

Aminoacylation assays were performed as previously described (Francklyn et al., 2008). The $tRNA^{Glu}$ was folded in water by heating at 80 °C for 2 min, 60 °C for 2 min, adding $MgCl_2$ (final concentration 10 mM), and incubating for 5 min at room temperature followed by incubation on ice for a minimum of 30 min. To initiate the reaction, ERS (100 nM) was added to 4 μM

$tRNA^{Glu}$ at 37°C in reaction cocktail (20 mM Tris pH 7.5, 20 mM KCl, 10 mM $MgCl_2$, 0.1 mg/mL BSA, 4 mM DTT, 4 mM ATP, 20 µM glutamic acid, 0.3 µCi/µL $^3$H-glutamic acid).

## Results and Discussion

*Section I: Protein Purification and Oligomerization Analysis*

We initially had difficulty purifying full-length ERS (aa. 1-687) due to the protein appearing in inclusion bodies (Figure 5B, right panel). We hypothesized that the linker region facilitates folding of ERS and solubilization of the protein since ERS exists *in vivo* with a linker joining it to PRS. Therefore, we designed two maltose-binding protein (MBP)-tagged extended ERS constructs: $ERS_{RC}$ and $ERS_{2.5W}$. The latter construct was designed based on a previous finding that $ERS_{2.5W}$ exists in cells as a caspase-3 cleavage product (Halawani et al., 2018). In addition, we included the small ubiquitin-like modifier (SUMO) solubility enhancer. These constructs are shown in Figure 5A. As shown in Figure 5B, the presence of the linker domain in the $ERS_{RC}$ and $ERS_{2.5W}$ constructs enhanced solubility of the protein and thereby facilitated protein purification. Though a few low-molecular weight impurities remained present after size-exclusion chromatography, the final proteins were estimated to be ~90% pure (Figure 5C).

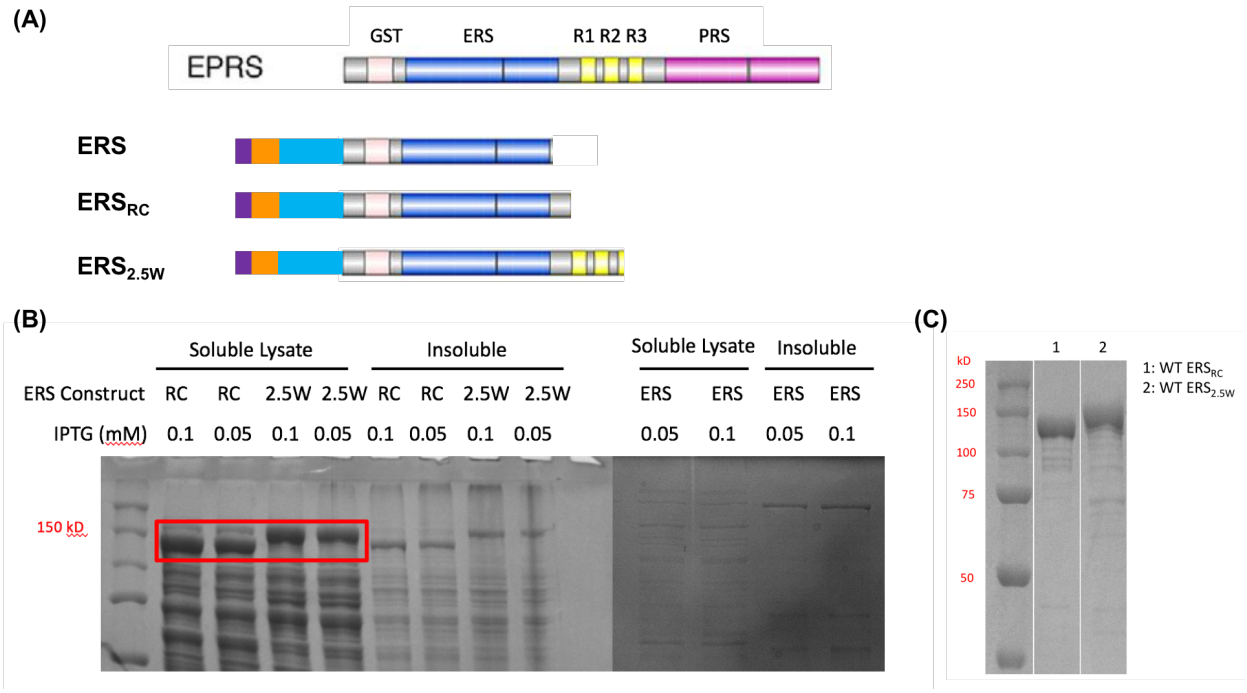


**Figure 5.** Inclusion of the linker domain in the WT ERS construct enhanced solubility of the protein, enabling purification. (A) ERS constructs, referenced to full-length EPRS. Tags: His-tag (purple), SUMO (orange), MBP (blue). (B) Proteins after IPTG induction at 16 °C overnight and lysis by sonication, shown on Coomassie-stained SDS-PAGE gels visualized with UV light. (C) Final purified proteins (4 µg). All proteins retained an N-terminal MBP-tag after purification.

To assess the oligomerization state of the ERS proteins in solution, we performed an SEC/MALS experiment. As shown in Figure 6, only a single peak was observed for each protein, indicating that both proteins exist as monomers in solution. Theoretical molecular weights (MW) for MBP-tagged ERS$_{2.5W}$ and ERS$_{RC}$ are ~ 146 kDa and 127 kDa, respectively. These are consistent with MWs calculated based on the retention volume (Figure 6). These results are also consistent with the expectation based on the known oligomeric state of class I synthetases (Bullwinkle & Ibba, 2014) and with models of the MSC, where although EPRS exists as a dimer through direct contact between the PRS domains, the ERS portion does not form a self-dimer (Cho et al., 2015) (see Figure 3).

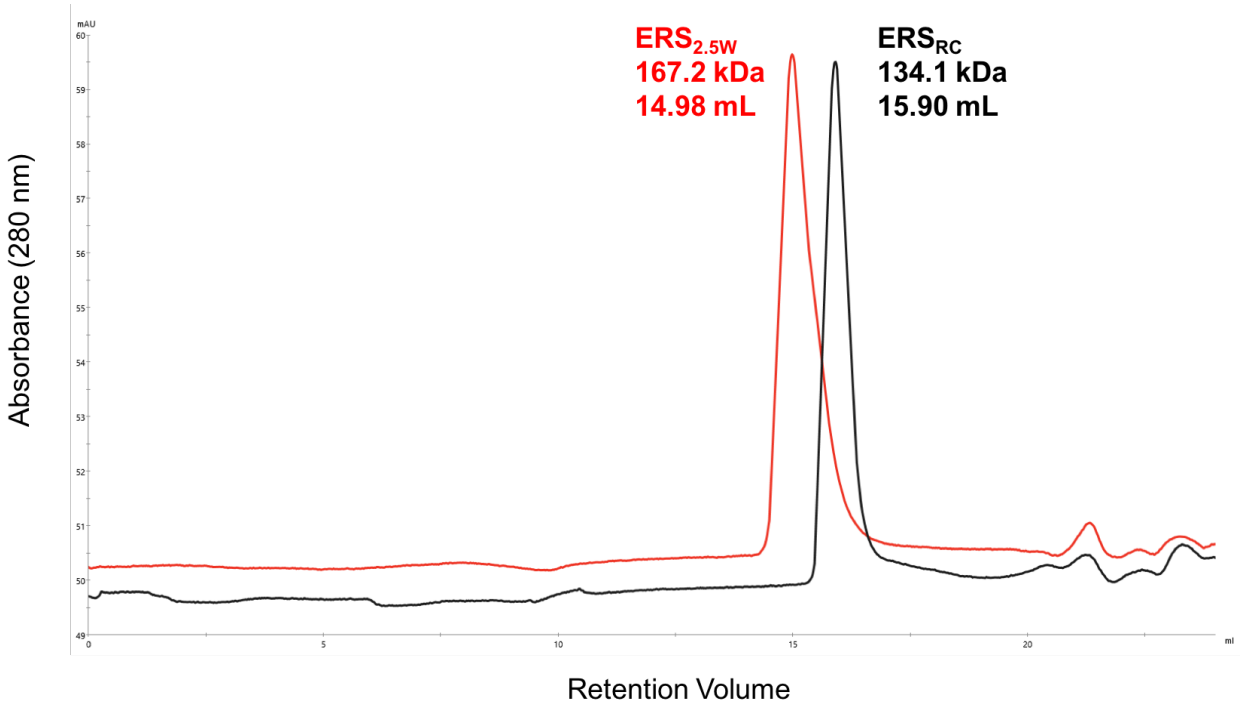


**Figure 6.** SEC/MALS chromatogram of purified WT $ERS_{2.5W}$ and $ERS_{RC}$. Both proteins exist as monomers in solution. MWs calculated from the retention volume are consistent with theoretical MWs for both $ERS_{2.5W}$ and $ERS_{RC}$. Experiment performed by Dr. William Cantara.

*Section II: Aminoacylation Activity*

As discussed in the introduction of this chapter, previously purified $ERS_{2.5W}$ displayed poor catalytic activity (Halawani et al., 2018). We next tested our purified WT ERS constructs to determine their aminoacylation activity. Results of these charging assays revealed that both $ERS_{RC}$ and $ERS_{2.5W}$ are active in $tRNA^{Glu}$ charging (Figure 7). We estimate that our proteins are 50 - 80 times more active in aminoacylation than the $ERS_{2.5W}$ preparation reported in Halawani et al (2018).

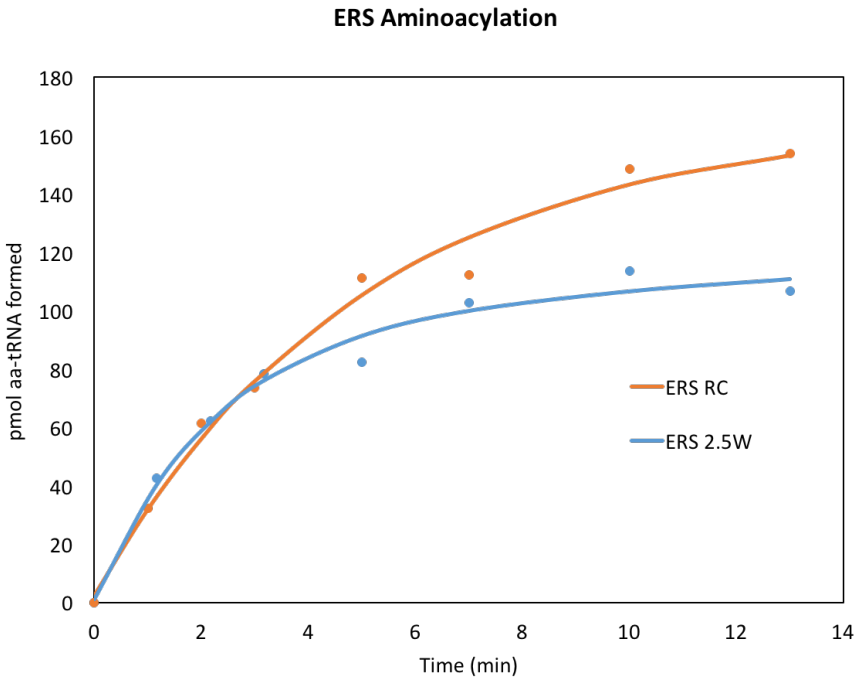


**Figure 7.** Both WT $ERS_{RC}$ and WT $ERS_{2.5W}$ are active in $tRNA^{Glu}$ charging. Experiment performed by Danni Jin.

Although WT $ERS_{RC}$ achieves a greater degree of product formation than $ERS_{2.5W}$, the slope for initial rate is nearly identical between the two proteins. This suggests that the two proteins have similar activities. A more detailed kinetic analysis is carried out in Chapter 2.

## Acknowledgements

I would like to thank Danni Jin for her assistance in the protein purification and for obtaining the aminoacylation data. I would like to thank Dr. William Cantara for performing the SEC/MALS experiments. Finally, I would like to thank Dr. Paul Fox and Dr. Kotaro Nakanishi for providing key plasmids.

# Chapter 2: Characterization of ERS Point Mutations Implicated in Human Disease

## Introduction

According to data from the Human Gene Mutation Database (HGMD), there are six total reported *EPRS* mutations that have been linked to disease. Mutation R339E is linked to autism spectrum disorder (Iossifov et al., 2014). Five other mutations—R339*, P1115R, M1126T, P1160S, and T1223Lfs3*[3]— are linked to hypomyelinating leukodystrophy and may be related to reduced translation ability through reduced protein availability, abnormal MSC assembly, and/or abnormal aminoacylation (Mendes et al., 2018).

Compound heterozygous *EPRS* mutations, P14R and E205G, were discovered by our collaborators in patients with type 1 diabetes and bone disease. Residue P14 is located in the GST domain, and E205 is in the catalytic domain. The location of these residues within the full-length domain structure of EPRS is shown in Figure 8.

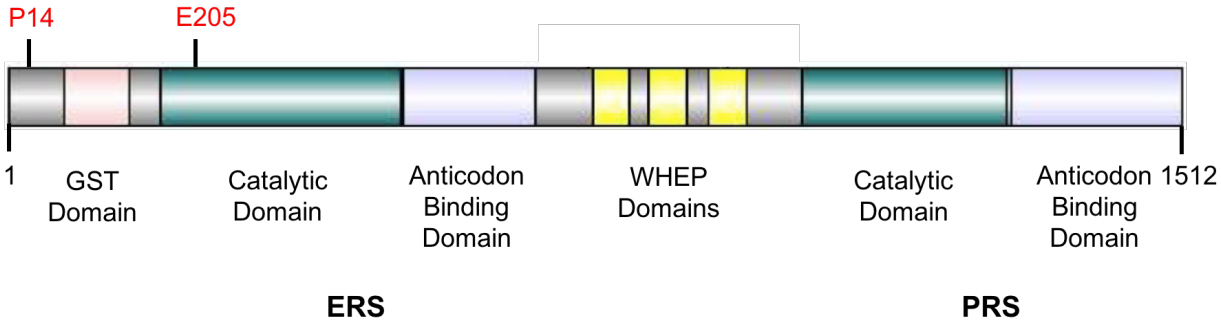


**Figure 8.** Full-length domain structure of EPRS highlighting residues P14 and E205. P14 lies in the GST domain, while E205 lies in the catalytic domain.

[3] R339* is a nonsense mutation, meaning the mutation introduces a premature stop codon (indicated by "*"). T1223Lfs3* is a frameshift mutation, where T at position 1223 is changed to L, and a stop codon is introduced 3 codons downstream.

This chapter will characterize these ERS point mutations, exploring sequence homology and measuring their effect on tRNA binding, aminoacylation, and amino acid activation.

## Materials and Methods

### *Phylogenetic Studies*

Multi-sequence alignments were generated using the Clustal Omega multiple sequence alignment tool. Sequences were obtained from the NCBI database. A homology model for ERS was created by Dr. William Cantara based on *E. coli* GlnRS using the ExPASy SWISS-MODEL server and edited with PyMOL software.

### *Plasmid Construction*

For details on cloning, see "Plasmid Construction" in Chapter 1. Mutagenesis for the P14R mutant, E205G mutant, and the double mutant P14R + E205G was accomplished using site-directed, ligase-independent mutagenesis (SLIM). Primers were designed by Danni Jin and the mutagenesis performed as described (Chiu et al., 2008). Mutations were confirmed by Sanger sequencing. All mutations were created in the context of the $ERS_{2.5W}$ construct. The E205G mutation was also created in the context of the $ERS_{RC}$ construct.

### *Protein Preparation*

For details on protein preparation, see "Protein Preparation" in Chapter 1.

### *RNA Preparation*

For details on RNA preparation, see "RNA Preparation" in Chapter 1.

*Fluorescent RNA Labeling*

The tRNA was labeled with fluorescein-5-thiosemicarbazide (FTSC) at the 3′ end as described (Rye-McCurdy et al., 2015). The concentration and labeling efficiency were determined by measuring the absorbance at 260 nm and 495 nm, using the following extinction coefficients: $\varepsilon_{495nm}$ = 85,000 $M^{-1}cm^{-1}$ (FTSC) and $\varepsilon_{260nm}$ = 60.4 × $10^4$ $M^{-1}cm^{-1}$ ($tRNA^{Glu}$).

*Fluorescence Anisotropy Binding Assays*

The 3′ FTSC-labeled $tRNA^{Glu}$ was folded in 50 mM Tris (pH 8) buffer by heating at 80 °C for 2 min, 60 °C for 2 min, adding $MgCl_2$ (final concentration 1 mM), and incubating for 5 min at room temperature followed by incubation on ice for a minimum of 30 min. The fluorescence anisotropy (FA) binding assays were then carried out as previously described (Rye-McCurdy et al., 2015). RNA (5 nM) was incubated with serially diluted ERS at room temperature for 30 min in FA binding buffer (20 mM Tris pH 8, 35 mM NaCl, 1 mM $MgCl_2$). The data were fit to the Hill equation and $K_d$ values were derived from three independent experiments.

*Aminoacylation Assays*

Aminoacylation assays were performed as previously described (Francklyn et al., 2008). For details on tRNA folding, see "Aminoacylation Assays" in Chapter 1. Assays were performed under $k_{cat}/K_M$ conditions with 25 nM $ERS_{2.5W}$ (WT) or 100 nM $ERS_{2.5W}$ (mutants P14R, E205G, and P14R + E205G) and 0.5 μM $tRNA^{Glu}$ at 37 °C in reaction cocktail (20 mM Tris pH 7.5, 20 mM KCl, 10 mM $MgCl_2$, 0.1 mg/mL BSA, 4 mM DTT, 4 mM ATP, 20 μM glutamic acid, 0.3 μCi/μL $^3$H-glutamic acid) for 2 min with time points every 20 sec.

To determine kinetic parameters $v_{max}$ and $K_M$, assays were performed with 100 nM $ERS_{2.5W}$ and $tRNA^{Glu}$ concentrations ranging from 0.25 - 8 μM (WT) or 0.5 - 16 μM (mutants). Time points were taken every 20 sec with a time course of 2 min.

*Preparation of Unchargeable tRNA*

To prepare a tRNA that could not be aminoacylated, the 3′ end of $tRNA^{Glu}$ was oxidized with sodium periodate ($NaIO_4$) as described (Rye-McCurdy et al., 2015). The oxidized tRNA was then stabilized by a two-step sequence of reactions (protocol courtesy of Dr. Craig Forsyth). First, the tRNA was reacted with 20-fold molar excess of benzylamine in 25 mM Tris-HCl pH 6.3 with intermittent vortexing at room temperature for 60 min. The tRNA was then reacted with 20-fold molar excess of sodium cyanoborohydride and vortexed intermittently at room temperature for 60 min. The RNA was purified with a Roche G-25 spin column and ethanol precipitated to yield the final 3′-end defective $tRNA^{Glu\text{-}ox}$ product.

*ATP-$PP_i$ Exchange Assays*

The amino acid activation step of the aminoacylation reaction was assessed using the ATP-$PP_i$ exchange assay (Francklyn et al., 2008). The tRNA was pre-bound to ERS by incubation at room temperature for 30 min. Reaction conditions were 20 mM Tris-HCl pH 7.5, 20 mM KCl, 10 mM $MgCl_2$, 4 mM DTT, 0.1 mg/mL BSA, 4 mM ATP, 2mM $PP_i$ + [$^{32}$P]-$PP_i$, 10 μM 3′-end defective $tRNA^{Glu\text{-}ox}$, 3 μM ERS, and 1.6 mM glutamic acid at 37 °C. Time points were taken every 6 min over a 30 min time course by quenching 2 μL of reaction into 8 μL of 200 mM NaOAc pH 5. Spots (2 μL) were placed on a TLC plate and eluted in 750 mM $KH_2PO_4$, 4 M urea, pH 3.5. Plates were exposed to a phosphor screen and visualized on a Typhoon scanner.

## Results and Discussion

*Section I: Sequence Conservation of the Mutated Residues*

We performed a sequence alignment to gain insight into the extent of conservation of the mutated residues. The multi-sequence alignment in Figure 9A demonstrates a high degree of conservation among eukaryotic species at the mutated residues.

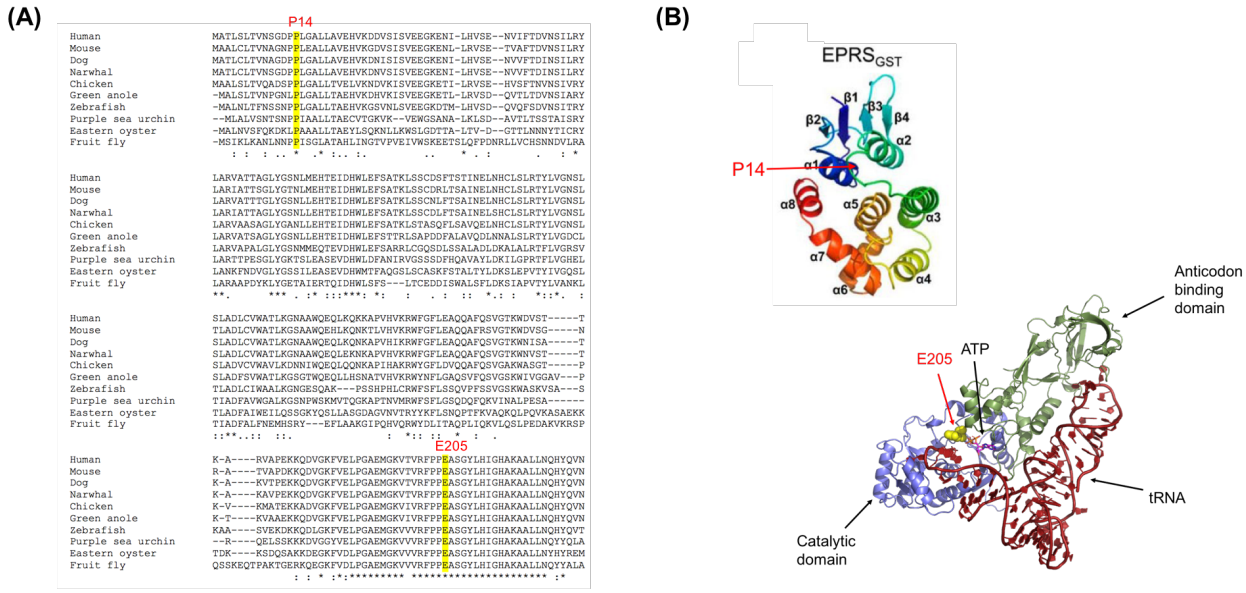


**Figure 9.** Sequence conservation of the mutated residues and their locations in human ERS. (A) Sequence alignment showing a high degree of conservation at residues P14 and E205 among a number of different eukaryotes. (B) Top: Location of the P14 residue in the GST domain. Image adapted from Cho et al., 2015. Bottom: Homology model of ERS domain based on *E. coli* GlnRS, showing E205 is localized to the ATP-binding pocket of the catalytic domain. Model sequence identity = 36%; sequence similarity = 38%. Model generated by Dr. William Cantara.

The high degree of conservation suggests that these amino acids are likely playing an important role in the function of the enzyme. If they are mutated, as in the case of the two patients reported to us, cellular and/or physiological function is likely to go awry. According to structures and sequence alignments of the EPRS GST domain, the P14 residue is located at the N-terminus of the

α1 helix (Cho et al., 2015) (Figure 9B, top panel). Previous phylogenetic analyses of GST domains in AARSs showed the GST domain to appear in ERS around the emergence of eukaryotes (Guo, Schimmel, & Yang, 2010). As GST domains facilitate protein folding and protein-protein interactions, we hypothesize that mutation of the P14 residue may play an important structural role in the folding of this domain and affect association of EPRS with the MSC. A homology model based on *E. coli* GlnRS reveals that the E205 residue is nestled within the ATP-binding pocket of the catalytic domain (Figure 9B, bottom panel). Given that the amino acid glycine lacks a side chain, it is possible that the E205G mutation widens the ATP-binding site, reducing the ATP binding affinity. Therefore, we hypothesize that the E205G mutation will have a negative impact on aminoacylation.

*Section II: tRNA Binding*

The binding of tRNA to AARS is a pivotal step in the charging of tRNA. We performed FA binding assays to study the binding of $tRNA^{Glu}$ to our ERS proteins. We first studied binding of WT $ERS_{RC}$ and $ERS_{2.5W}$ to $tRNA^{Glu}$, as this would provide insight into whether our constructs would be effective for study of the P14R and E205G point mutations. As seen by the graphs in Figure 10A-B and the table in Figure 10F, WT $ERS_{2.5W}$ bound $tRNA^{Glu}$ with approximately 4-fold greater affinity than WT $ERS_{RC}$. This suggests that the WHEP domains of EPRS play a role in facilitating $tRNA^{Glu}$ binding.

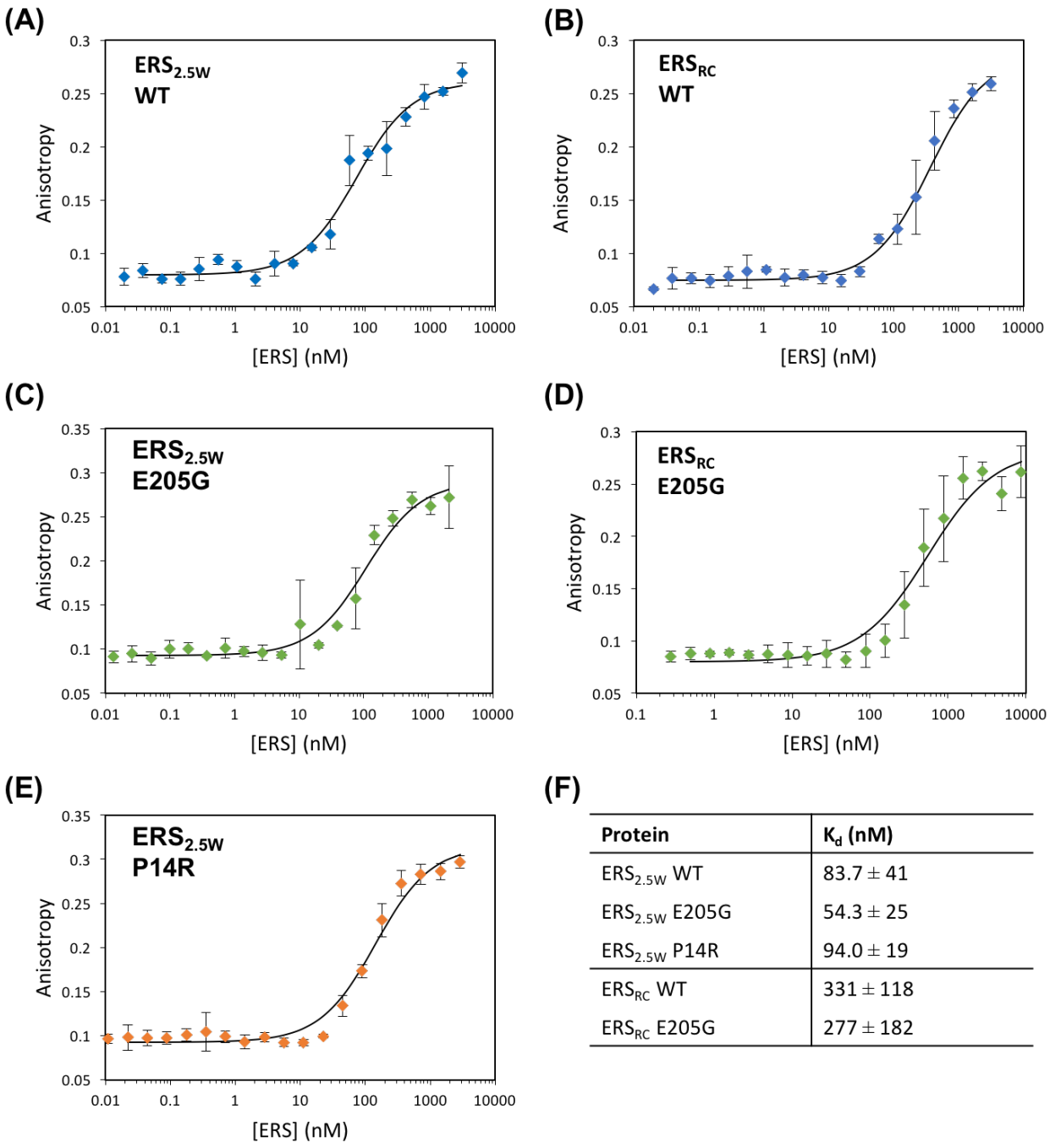


(F)

| Protein | $K_d$ (nM) |
|---|---|
| $ERS_{2.5W}$ WT | 83.7 ± 41 |
| $ERS_{2.5W}$ E205G | 54.3 ± 25 |
| $ERS_{2.5W}$ P14R | 94.0 ± 19 |
| $ERS_{RC}$ WT | 331 ± 118 |
| $ERS_{RC}$ E205G | 277 ± 182 |

**Figure 10.** Fluorescence anisotropy assays measuring binding of $tRNA^{Glu}$ to WT and mutant ERS constructs. (A) $ERS_{2.5W}$ WT, (B) $ERS_{RC}$ WT, (C) $ERS_{2.5W}$ E205G, (D) $ERS_{RC}$ E205G, (E) $ERS_{2.5W}$ P14R, (F) Table summarizing $K_d$ values for all proteins.

It is known that WHEP domains can bind RNA. For example, the WHEP domains of EPRS have previously been shown to bind the GAIT element RNA (Jia et al., 2008). In addition, purified EPRS linker is able to bind $tRNA^{Lys}$ (Jia et al., 2008). It is also known that the WHEP domain of MetRS has a tRNA-sequestering function (Kaminska et al., 2001). The linker region of EPRS is highly basic, and it is likely that it interacts with tRNAs non-specifically. Thus, it is likely that the presence of 2.5 WHEP domains facilitates the binding of $tRNA^{Glu}$ to ERS by increasing the total local concentration of tRNA. This hypothesis of non-specific interaction could be tested by performing FA binding assays with noncognate tRNA.

Having established that WT $ERS_{2.5W}$ binds $tRNA^{Glu}$ with greater affinity than $ERS_{RC}$, we created the P14R and E205G point mutations within the context of the $ERS_{2.5W}$ construct and performed additional FA binding assays. As neither mutation lies within the anticodon binding domain, we hypothesized that the mutations would not affect tRNA binding affinity. As seen in Figure 10C, E, and F, our results indicate that indeed neither mutation has an effect on $tRNA^{Glu}$ binding, as both the $ERS_{2.5W}$ P14R and $ERS_{2.5W}$ E205G mutants bind $tRNA^{Glu}$ with the same affinity as their WT counterpart. It is important to note that the N-terminal MBP tag may alter tRNA binding affinity so that the reported $K_d$ values do not reflect absolute physiological values; however, all constructs maintain the MBP tag, so comparisons between the constructs are still valid. In addition, the $K_d$ values found for the $ERS_{2.5W}$ constructs are comparable to previous values determined for untagged *E. coli* ERS (Chongdar et al., 2015).

We also performed FA binding experiments with an $ERS_{RC}$ E205G mutant. As seen in Figure 10D and 10F, this protein bound $tRNA^{Glu}$ with the same affinity as WT $ERS_{RC}$. The implication of this result is two-fold. First, this result supports our earlier data that the presence of the E205G mutation does not affect $tRNA^{Glu}$ binding affinity. Second, even though the E205G

mutation is present in this construct, the protein still bound $tRNA^{Glu}$ with lower affinity than when 2.5 WHEP domains are present. Thus, this data supports our observation that the presence of 2.5 WHEP domains in ERS enhances $tRNA^{Glu}$ binding.

*Section III: Aminoacylation*

As described earlier, both WT $ERS_{RC}$ and $ERS_{2.5W}$ are active in $tRNA^{Glu}$ charging, with similar activities (see Figure 7). We next studied the aminoacylation activity of the ERS mutants. We hypothesized that the E205G mutation, but not P14R, would contribute to a defect in aminoacylation. As P14 lies in the GST domain, it is unlikely to affect aminoacylation. In contrast, E205 lies in the ATP binding pocket of the catalytic domain, likely playing a role in the enzyme's catalytic function.

To gain an initial indication of the enzymes' activities, we performed aminoacylation assays under $k_{cat}/K_M$ conditions (A more detailed kinetic analysis is described below). At low substrate concentrations ($[S] << K_M$), the initial rate of reaction is proportional to $k_{cat}/K_M$. We performed assays at 0.5 μM $tRNA^{Glu}$ to achieve these conditions. As shown in the initial rate data plotted in Figure 11A, the P14R mutant displays near-WT aminoacylation activity, whereas the E205G variant has a severe aminoacylation defect. Results of these assays are summarized in Figure 11B. As demonstrated by the comparisons in fold decrease of $k_{cat}/K_M$, the E205G mutation—whether as a single mutation or in combination with P14R as a double mutant—significantly reduces aminoacylation activity. These results are consistent with our hypothesis.

(A)

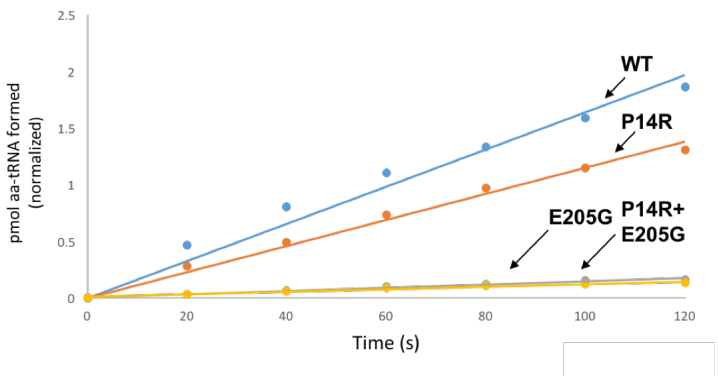


(B)

| ERS Construct | $K_{cat}/K_M$ ($mM^{-1}$ $s^{-1}$) | Fold Decrease |
|---|---|---|
| WT | 86.2 ± 29 | —— |
| P14R | 59.6 ± 26 | 1.4 |
| E205G | 7.60 ± 1.7 | 11 |
| P14R + E205G | 5.73 ± 1.9 | 15 |

**Figure 11.** Aminoacylation activities of $ERS_{2.5W}$ WT and mutants. (A) Aminoacylation assays performed under $k_{cat}/K_M$ conditions with 25 – 100 nM enzyme and 0.5 µM $tRNA^{Glu}$. N = 3 or 4. (B) Summary table of kinetic results. $ERS_{2.5W}$ P14R has near-WT aminoacylation activity, while $ERS_{2.5W}$ E205G has a severe aminoacylation defect.

Again, it is important to note that activities of these proteins may be altered due to the presence of the N-terminal MBP tag. However, WT ERS is still active with the MBP tag (Figure 7, Figure 11). Furthermore, the calculated $k_{cat}/K_M$ for WT $ERS_{2.5W}$ is actually comparable to that of previously purified untagged ERS of *E. coli* (Sylvers et al., 1993), *Pseudomonas aeruginosa* (Hu et al., 2015), and rice (*Oryza sativa*) (Yang et al., 2018). In addition, all of the ERS constructs compared in Figure 11 maintain the MBP tag, so even if the determined parameters do not reflect absolute physiological values, the relative values are still valid, allowing us to assess the effects of the mutations on aminoacylation.

We also performed preliminary aminoacylation reactions at varying $tRNA^{Glu}$ concentration to determine kinetic parameters $v_{max}$ and $K_M$ for each of the enzymes. Results of these assays are shown in Figure 12 A-D.

(A)

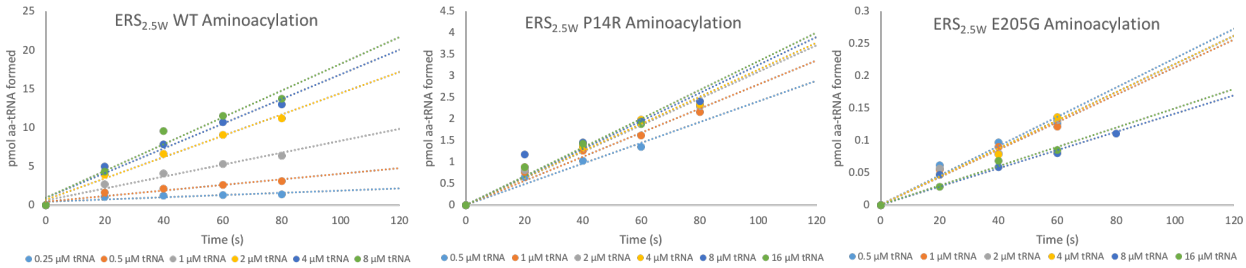


(B)

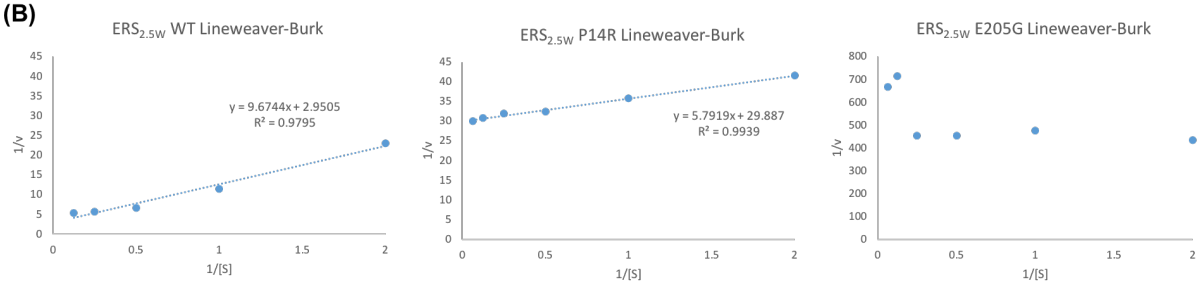


(C)

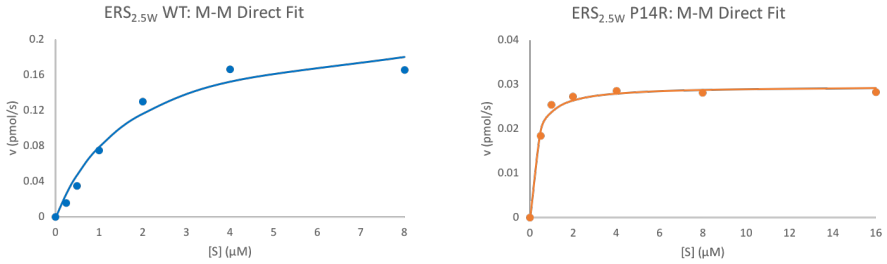


(D)

| ERS Construct | $V_{max}$ (pmol/s) | $K_M$ (µM) | $V_{max}/K_M$ |
|---|---|---|---|
| WT | 0.220 | 1.79 | 0.123 |
| P14R | 0.030 | 0.245 | 0.122 |

**Figure 12.** (A) Preliminary aminoacylation assays at varying $tRNA^{Glu}$ concentration to determine kinetic paramters for each of the enzymes. For WT $ERS_{2.5W}$, $tRNA^{Glu}$ was varied from 0.25 - 8 µM, while $tRNA^{Glu}$ was varied from 0.5 - 16 µM for $ERS_{2.5W}$ P14R and $ERS_{2.5W}$ E205G. (B) Inverse reciprocal plots for the aminoacylation reactions shown in A. (C) Direct fits to the Michaelis-Menten equation. (D) Summary of kinetic parameters obtained for $ERS_{2.5W}$ WT and $ERS_{2.5W}$ P14R based on the fits shown in panel C. Experiments performed by Danni Jin.

As shown in Figure 12A, the concentration range used for $tRNA^{Glu}$ (0.25 - 16 µM) was suitable for WT $ERS_{2.5W}$ but not ideal for $ERS_{2.5W}$ P14R and $ERS_{2.5W}$ E205G. In particular, for $ERS_{2.5W}$ P14R, the reaction rates for 2-16 µM $tRNA^{Glu}$ were nearly identical. This suggests that the reaction rate begins to plateau at approximately 2 µM $tRNA^{Glu}$, approaching $v_{max}$, and thus the

$K_M$ lies below this value. Lineweaver-Burk plots are shown in Figure 12B. Since linearization-based approaches can be subject to high degrees of error, we also fit the kinetic data directly to the Michaelis-Menten equation, $v = \frac{v_{max}[S]}{K_M+[S]}$ (Figure 12C). From this fit, we obtained kinetic parameters for WT $ERS_{2.5W}$ and $ERS_{2.5W}$ P14R, but the data was too poor to do so for $ERS_{2.5W}$ E205G.

Figure 12D compares the preliminary assay results for WT and P14R $ERS_{2.5W}$ (1 trial). Although the individual parameters are different, the values of $v_{max}/K_M$ are nearly identical for WT and P14R, which suggests that the two enzymes have similar catalytic efficiency. Based on these preliminary data, we conclude that the P14R mutation does not significantly affect catalytic efficiency for the aminoacylation reaction. However, more trials need to be performed in order to confirm this observation.

Of note, the calculated $K_M$ for $ERS_{2.5W}$ P14R shown in Figure 12D is quite low. If $K_M$ for $ERS_{2.5W}$ P14R is confirmed to be this low after further trials, the results in Figure 11 A-B are called into question. Those results depend on [S] << $K_M$, and 0.5 μM $tRNA^{Glu}$ is not low enough to achieve this condition for $ERS_{2.5W}$ P14R if it has a $K_M$ < 0.3 μM.

*Section IV: Amino Acid Activation*

Aminoacyl-tRNA synthetases catalyze aminoacylation of tRNA in two steps. The first step is the formation of an aminoacyl adenylate complex, and the second is the attachment of the amino acid to tRNA (see "Introduction," Figure 1). The ATP-$PP_i$ exchange assay is designed to measure enzyme activity by quantitating the reversible first step in this process. $^{32}$P-$PP_i$ is included in the assay mixture and in the presence of AARS is converted into $^{32}$P-ATP.

Unlike most AARSs, ERS, along with GlnRS, ArgRS, and class I LysRS, requires the presence of tRNA for the amino acid activation step. This poses a challenge for the assay because the presence of chargeable tRNA interferes with the assay. Chargeable tRNA will accept an amino acid transferred from aa-AMP, thereby depleting aa-AMP from the system and shifting the equilibrium for the activation reaction. Thus, it was important to generate a tRNA that did not get charged but that could still facilitate the amino acid activation reaction.

A previous study of *E. coli* GlnRS designed a suitably modified $tRNA^{Gln}$ through use of a modified synthetic tRNA, ligating chemically synthesized tRNA half-molecules to form $tRNA^{Gln}_{2'H}$ (Gruic-Sovulj et al., 2005). After trying multiple methods, we decided to use a $tRNA^{Glu}$ with its 3′ end oxidized with sodium periodate and stabilized with benzylamine and sodium cyanoborohydride. An outline of the reaction is provided in Figure 13A. A charging assay confirmed that this modified tRNA—$tRNA^{Glu\text{-}ox}$—was defective in tRNA charging (Figure 13B).

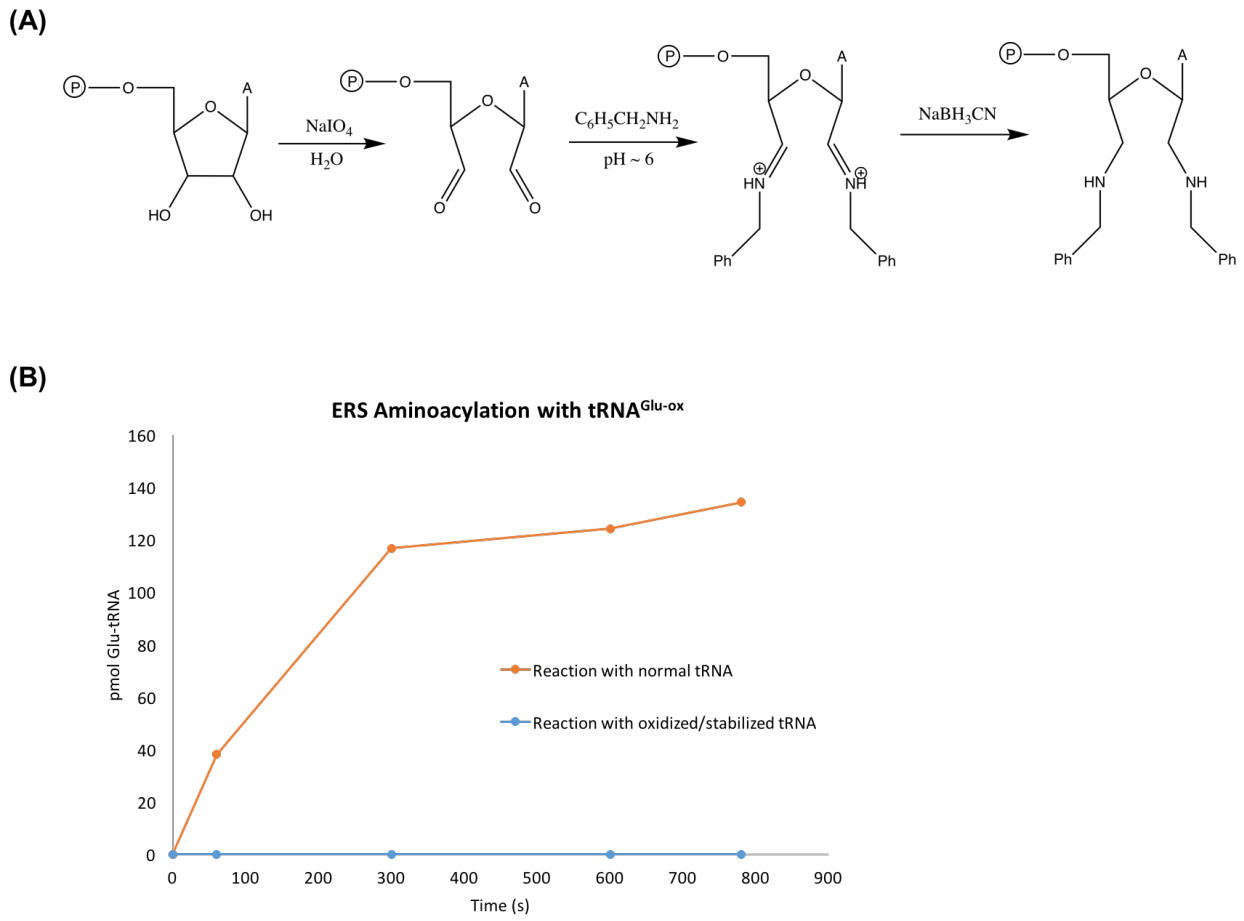


**Figure 13.** (A) Reaction scheme for oxidizing and stabilizing the 3′ terminal adenosine, A76, of $tRNA^{Glu}$. (B) A charging assay revealed that $tRNA^{Glu\text{-}ox}$ is defective for aminoacylation.

As seen in Figure 14, WT $ERS_{2.5W}$ displayed amino acid activation, consistent with previous trials. However, both the E205G and P14R mutant were defective in amino acid activation and activity could not be detected under the conditions of this assay.

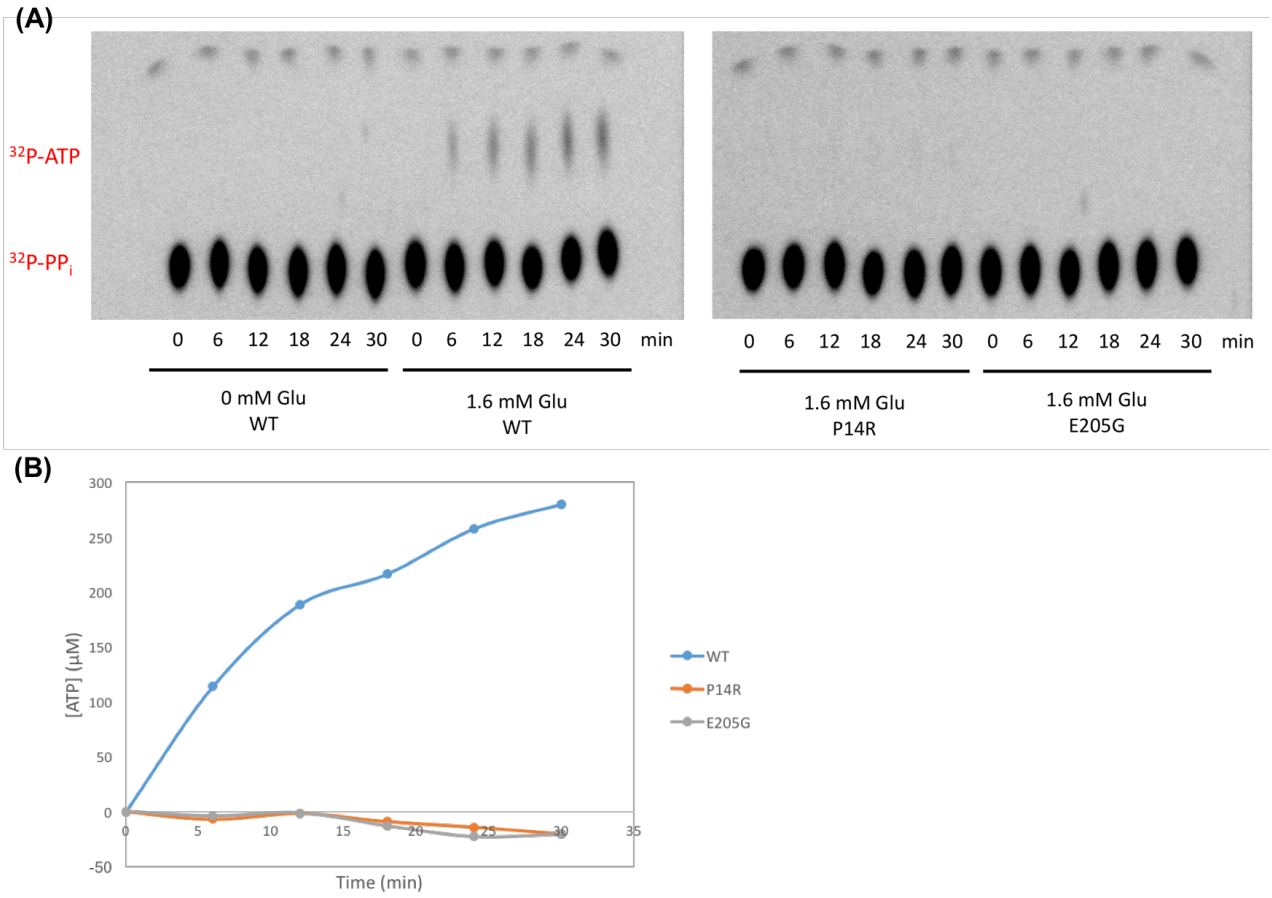


**Figure 14.** ATP-$PP_i$ exchange assay with WT and mutant $ERS_{2.5W}$. (A) WT $ERS_{2.5W}$ was active in amino acid activation, but mutant P14R and E205G $ERS_{2.5W}$ were not. Assays were performed with 3 μM $ERS_{2.5W}$ and 10 μM $tRNA^{Glu\text{-}ox}$. (B) Formation of ATP is nearly linear for WT $ERS_{2.5W}$ but completely defective for P14R and E205G mutants. Plots were generated by quantifying the phosphor transfer image of the TLC plates shown in panel A. Plot courtesy of Danni Jin.

The result of this assay for E205G was consistent with our hypothesis, as E205 is proposed to be located in the ATP-binding pocket and the mutation likely abrogates the enzyme's ability to interact with ATP. However, the result for P14R was surprising. Even though P14R does not significantly affect aminoacylation, it appears to be having an effect on amino acid activation. This deficiency in activation could perhaps be the explanation for the very slight defect in aminoacylation seen in Figure 11A-B. Plots obtained by quantification of the phosphor transfer

show that the amount of $^{32}$P-ATP synthesized increased substantially in the presence of WT $ERS_{2.5W}$ (Figure 14B). These results are comparable to those in ATP-$PP_i$ exchange assays performed with *E. coli* GlnRS (Uter et al., 2005). No ATP was formed in the presence of the P14R and E205G mutants, however. It is likely that sensitivity for this assay was not high enough to detect whatever activation may be occurring in the P14R mutant.

Previous unpublished data from our lab demonstrate cases where LysRS mutants, although displaying robust aminoacylation activity, appear defective in amino acid activation when studied with the ATP-$PP_i$ exchange assay. Therefore, although our result is unusual, it is not completely unprecedented. Under steady-state kinetic conditions, the rate-limiting step for class I AARSs is product (aminoacyl-tRNA) release (Zhang et al., 2006). That may help explain the discrepancy between the aminoacylation and amino acid activation results for the $ERS_{2.5W}$ P14R mutant. If there is a difference in kinetics between WT and P14R at the activation step, that would not be evident in the aminoacylation assay, as the rate-limiting step informing kinetic parameters is product release, not activation. When the assay is restricted to observing the activation step, as with the ATP-$PP_i$ exchange assay, then differences in $k_{cat}$ may become more readily apparent.

## Acknowledgements

I would like to thank our collaborators, Dr. Ron Wek and Dr. Orly Elpeleg, for sharing the patient data with us. I am grateful to Dr. William Cantara for constructing the homology model. I would like to thank Danni Jin for her assistance in obtaining data for the aminoacylation assays and quantification of phosphor transfer in the ATP-$PP_i$ exchange assays. I would also like to thank Dr. Craig Forsyth for his assistance in developing a protocol to stabilize oxidized $tRNA^{Glu}$. Finally,

I would like to thank Dr. Marina Bakhtina for her help in developing a protocol for the ATP-$PP_i$ exchange assays.

## Conclusions and Future Directions

In this work, we successfully purified recombinant human ERS and showed that it was active in aminoacylation with the oligomerization state in solution in agreement with other class I synthetases and with proposed structures for the MSC. We found that the presence of 2.5 WHEP domains increased protein solubility and enhanced $tRNA^{Glu}$ binding. We have shown the residues P14 and E205 to be highly conserved, indicating an important role in the functioning of the enzyme. Neither the P14R nor the E205G mutation affects $tRNA^{Glu}$ binding affinity. The E205G mutation, but not P14R, contributes to a defect in aminoacylation. While the E205G mutant is defective in amino acid activation, the P14R mutant is surprisingly defective in this as well. Taking these findings all together, the disease phenotypes observed in the patients may be linked to a defect in tRNA charging due to the E205G mutation. The exact role of the P14R mutation remains unclear and requires further study.

Unpublished data from our lab has shown that a P14R mutant displays increased proteolysis in HEK293T cells relative to the WT protein or the E205G variant, with a significantly increased amount of a C-terminal fragment with MW ~60 kDa observed. This demonstrates that the P14R mutation may contribute to a long-range structural effect. Therefore, it is possible that conformational changes induced by the P14R mutation could have a rate-limiting effect on the amino acid activation step.

In our future work, we plan to investigate folding of a WT and P14R mutant of an ERS GST construct through circular dichroism (CD) spectroscopy. To examine possible long-range effects of this mutation, we will also perform CD studies of the WT and P14R $ERS_{2.5W}$ proteins. In addition, we plan to perform rescue experiments for a cell proliferation defect in EPRS knockdown cells with WT and mutants. In collaboration with Dr. Ron Wek (Indiana University),

we plan to perform western blotting experiments to determine if truncated EPRS exists in patient cells, and to assess levels of uncharged $tRNA^{Glu}$ in patient cells. Finally, the primary noncanonical pathway we plan to investigate is how these mutations affect the integrated stress response (ISR).

In response to diverse stress stimuli, cells activate the ISR to restore homeostasis. The key feature of the ISR is phosphorylation of eukaryotic translation initiation factor 2 alpha (eIF2α) by an eIF2α kinase. There are four different types of eIF2α kinases, and each responds to distinct environmental and physiological stresses (Pakos-Zebrucka et al., 2016). General control nonderepressible 2 (GCN2) is an eIF2α kinase that is activated in response to amino acid starvation. Protein kinase R (PKR)-like endoplasmic reticulum kinase (PERK) is another eIF2α kinase, but is activated in response to endoplasmic reticulum (ER) stress resulting from accumulation of unfolded proteins (Pakos-Zebrucka et al., 2016). Although the ISR is generally a pro-survival, homeostatic program, severe stress can drive signaling toward cell death.

We hypothesize that the EPRS mutants sensitize cells to stress, leading to higher levels of the ISR that can diminish cell viability. A defect in ERS aminoacylation leads to accumulation of uncharged $tRNA^{Glu}$, which is analogous to amino acid starvation. Thus, in the case of the E205G mutation, the ISR is likely stimulated through activation of GCN2. The P14R mutation is likely to have an effect on protein folding, and we therefore propose that this mutation induces the ISR through activation of PERK. This hypothesis is summarized in Figure 15. This is certainly a possibility for disease etiology, as ER stress and activation of PERK have been implicated in autoimmune-mediated β-cell destruction in type 1 diabetes (Zhong et al., 2012). Alternatively, P14R may contribute to disease through the mammalian target of rapamycin (mTOR) signaling pathway. The mTOR pathway serves as a key regulator for cellular growth, metabolism, proliferation, and survival (Laplante & Sabatini, 2009). The mTOR complex 1 (mTORC1) works

together with protein kinase S6 kinase 1 (S6K1) in the mTORC1-S6K1 axis. EPRS is known to be phosphorylated by mTORC1-S6K1, which releases EPRS from the MSC to facilitate fatty acid uptake (Arif et al., 2017). Prolonged ER stress activates mTORC1 (Guan et al., 2013); therefore, it is possible that this activation of mTORC1 also leads to inducible release of EPRS from the MSC. If the P14R mutation affects association of EPRS with the MSC, this potential interaction with mTORC1 could be dysregulated, creating downstream effects that lead to disease.

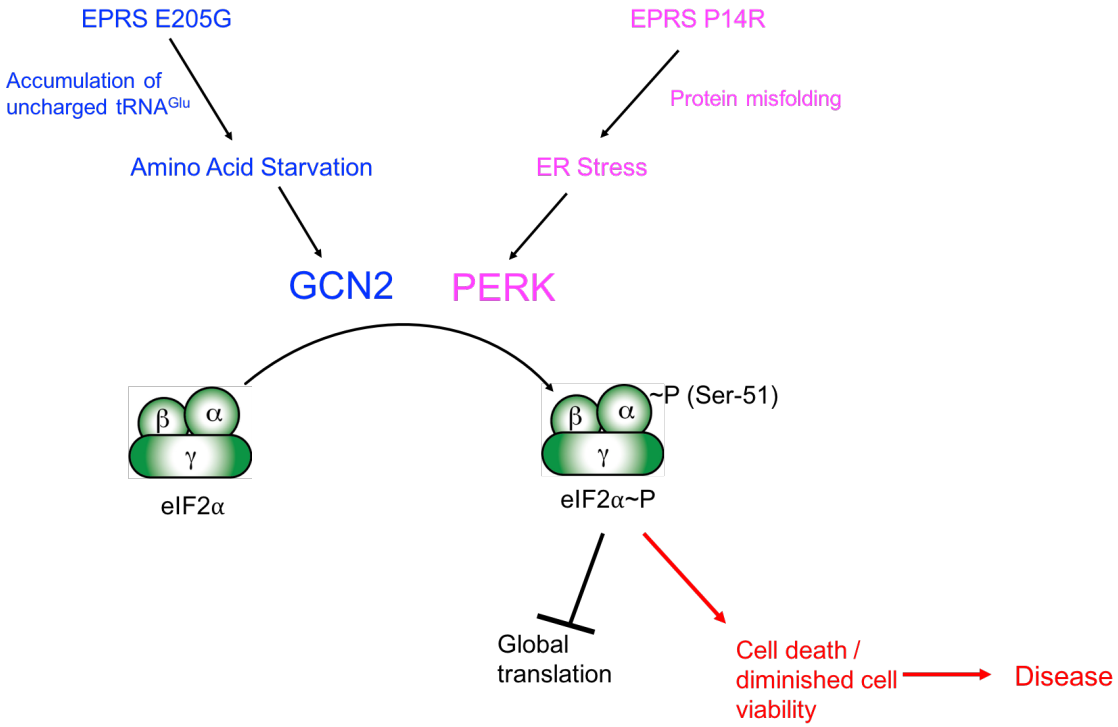


**Figure 15.** Hypothesis of the integrated stress response (ISR) pathway to disease from EPRS mutations E205G and P14R. E205G may lead to accumulation of uncharged $tRNA^{Glu}$, causing amino acid starvation, and activation of GCN2. P14R may lead to protein misfolding, causing ER stress and activation of PERK. Both GCN2 and PERK phosphorylate eIF2α, initiating the ISR. This leads to a decrease in global translation, and with severe enough stress, this may lead to diminished cell viability and disease.

## References


Arif, A., & Fox, P.L. (2017). Unexpected metabolic function of a tRNA synthetase. *Cell Cycle*, *16*(23), 2239–2240.

Arif, A., Jia, J., Mukhopadhyay, R., Willard, B., Kinter, M., & Fox, P.L. (2009). Two-site phosphorylation of EPRS coordinates multimodal regulation of noncanonical translational control activity. *Molecular Cell*, *35*(2), 164–180.

Arif, A., Terenzi, F., Potdar, A.A., Jia, J., Sacks, J., China, A., … Fox, P.L. (2017). EPRS is a critical mTORC1-S6K1 effector that influences adiposity in mice. *Nature*, *542*(7641), 357–361.

Arnez, J.G., & Moras, D. (1997). Structural and functional considerations of the aminoacylation reaction. *Trends in Biochemical Sciences*, *22*(6), 211–216.

Bullwinkle, T.J., & Ibba, M. (2014). Emergence and evolution. *Topics in Current Chemistry*, *344*, 43–87.

Bult, C.J., White, O., Olsen, G.J., Zhou, L., Fleischmann, R.D., Sutton, G.G., … Venter, J.G. (1996) Complete genome sequence of the methanogenic archaeon, Methanococcus jannaschii. *Science*, *273*(5278), 1058–1073.

Cahuzac, B., Berthonneau, E., Birlirakis, N., Guittet, E., & Mirande, M. (2000). A recurrent RNA-binding domain is appended to eukaryotic amino- acyl-tRNA synthetases. *EMBO Journal*, *19*(3), 445–452.

Chiu, J., Tillett, D., Dawes, I.W., & March, P.E. (2008). Site-directed, ligase-independent mutagenesis (SLIM) for highly efficient mutagenesis of plasmids greater than 8kb. *Journal of Microbiological Methods*, *73*(2), 195–198.

Cho, H.Y., Maeng, S.J., Cho, H.J., Choi, Y.S., Chung, J.M., Lee, S., … Kim, S. (2015). Assembly of multi-tRNA synthetase complex via heterotetrameric glutathione transferase-homology domains. *Journal of Biological Chemistry*, *290*(40), 29313–29328.

Chongdar, N., Dasgupta, S., Datta A.B., & Basu, G. (2015). Dispensability of zinc and the putative zinc-binding domain in bacterial glutamyl-tRNA synthetase. *Bioscience Reports*, *35*(2), 1–13.

Eriani, G., Celarue, M., Poch, O., Gangloff, J., & Moras D. (1990). Partition of tRNA synthetases into two classes based on mutually exclusive sets of sequence motifs. *Nature*, *347*(6289), 203–206.

Francklyn, C.S., First, E.A., Perona, J.J., & Hou, Y.M. (2008). Methods for kinetics and thermodynamic analysis of aminoacyl-tRNA synthetases. *Methods*, *44*(2), 100–118.

Froelich, C.A., & First, E.A. (2011). Dominant Intermediate Charcot-Marie-Tooth disorder is not due to a catalytic defect in tyrosyl-tRNA synthetase. *Biochemistry*, *50*(33), 7132–7145.

Gruic-Sovulj, I., Uter, N., Bullock, T., & Perona, J.J. (2005). tRNA-dependent aminoacyl-adenylate hydrolysis by a nonediting class I aminoacyl-tRNA synthetase. *Journal of Biological Chemistry*, *280*(25), 23978–23986.

Guan, B.J., Drokowski, D., Majumder, M., Schmotzer, C.L., Kimball, S.R., Merrick, W.C., Koromilas, A.E., & Hatzoglou, M. (2014). *Journal of Biological Chemistry*, *289*(18), 12593–12611.

Guo, M., & Yang, X.L. (2014). Architecture and metamorphosis. *Topics in Current Chemistry*, *344*, 89–118.

Guo, M., Schimmel, P., & Yang, X.L. (2010). Functional expansion of human tRNA synthetases achieved by structural interventions. *FEBS Letters*, *584*(2), 434–442.

Guo, M., Yang, X.L., & Schimmel, P. (2010). New functions of aminoacyl-tRNA synthetases beyond translation. *Nature Reviews Molecular Cell Biology*, *11*(9), 668–674.

Halawani, D., Gogonea, V., DiDonato, J.A., Pipich, V., Yao, P., China, A., … Fox, P.L. (2018). Structural control of caspase-generated glutamyl-tRNA synthetase by appended noncatalytic WHEP domains. *Journal of Biological Chemistry*, *293*(23), 8843–8860.

Han J.M., Jeong S.J., Park M.C., Kim G., Kwon N.H., Kim H.K., … Kim S. (2012). Leucyl-tRNA synthetase is an intracellular leucine sensor for the mTORC1-signaling pathway. *Cell*, *149*(2), 410–424.

Havrylenko, S., & Mirande, M. (2015). Aminoacyl-tRNA synthetase complexes in evolution. *International Journal of Molecular Sciences*, *16*(3), 6571–6594.

Hu, Y., Guerrero, E., Keniry, M., Manrrique, J., & Bullard, J.M., (2015). Identification of chemical compounds that inhibit the function of glutamyl-tRNA synthetase from Pseudomonas aeruginosa. *Journal of Biomolecular Screening*, *20*(9), 1160–1170.

Ibba, M., Becker, H.D., Stathopoulos, C., Tumbula, D.L, & Söll, D. (2000). The adapter hypothesis revisited. *Trends in Biochemical Sciences*, *25*(7), 311–316.

Ibba, M., & Söll, D. (2000). Aminoacyl-tRNA synthesis. *Annual Review of Biochemistry*, *69*(1), 617–650.

Iossifov, I., O'Roak, B.J., Sanders, S.J., Ronemus, M., Krumm, N., Levy D., … Wigler, M. (2014). The contribution of de novo coding mutations to autism spectrum disorder. *Nature*, 515(7526), 216–221.

Jia, J., Arif, A., Ray, P.S., & Fox, P.L. (2008). WHEP domains direct noncanonical function of glutamyl-prolyl tRNA synthetase in translational control of gene expression. *Molecular Cell*, *29*(6), 679–690.

Kaminska, M., Shalak, V. & Mirande, M. (2001). The appended C-domain of human methionyl-tRNA synthetase has a tRNA-sequestering function. *Biochemistry*, *40*(47), 14309–14316.

Kim, J.H., Han, J.M., & Kim, S. (2014) Protein-protein interactions and multi-component complexes of aminoacyl-tRNA synthetases. *Topics in Current Chemistry*, *344*, 119–144.

Kim, J.Y., Kang, Y.S., Lee, J.W., Kim, H.J., Ahn, Y.H., Park, H., Ko, Y.G., & Kim, S. (2002). p38 is essential for the assembly and stability of macromolecular tRNA synthetase complex: implications for its physiological significance. *Proceedings of the National Academy of Sciences in the United States of America*, *99*(12), 7912–7916.

Kisselev, L.L. & Wolfson, A.D. (1994). Aminoacyl- tRNA synthetases from higher eukaryotes. *Progress in Nucleic Acid Research and Molecular Biology*, *48*, 83–142.

Ko, Y.G., Kang, Y.S., Kim, E.K., Park, S.G., & Kim, S. (2000). Nucleolar localization of human methionyl–tRNA synthetase and its role in ribosomal RNA synthesis. *Journal of Cell Biology*, *149*(3), 567–574.

Koonin, E.V., Mushegian, A.R., Tatusov, R.L., Altschul, S.F., Bryant, S.H., Bork, P., & Valencia, A. (1994). Eukaryotic translation elongation factor lγ contains a glutathione transferase domain: Study of a diverse, ancient protein superfamily using motif search and structural modeling. *Protein Science*, *3*(11), 2045–2054.

Laplante, M., & Sabatini, D.M. (2009). mTOR signaling at a glance. *Journal of Cell Science*, *122*, 3589–3594.

Laporte, D., Huot, J.L., Bader, G., Enkler, L., Senger, B., & Becker, H.D. (2014). Exploring the evolutionary diversity and assembly modes of multi-aminoacyl-tRNA synthetase complexes: Lessons from unicellular organisms. *FEBS Letters*, *588*(23), 4268–4278.

Lee, E.Y., Lee, H.C., Kim, H.K., Jang, S.Y., Park, S.J., Kim, Y.H., … & Kim, M.H. (2016). Infection-specific phosphorylation of glutamyl- prolyl tRNA synthetase induces antiviral immunity. *Nature Immunology*, *17*(11), 1252–1262.

Lee, S.W., Cho, B.H., Park, S.G., & Kim, S. (2004). Aminoacyl-tRNA synthetase complexes: beyond translation. *Journal of Cell Science*, *117*, 3725-3734.

Lei, H.Y., Zhou, X.L., Ruan, Z.R., Sun, W.C., Eriani, G., & Wang, E.D. (2015). Calpain cleaves most components in the multiple aminoacyl-tRNA synthetase complex and affects their functions. *Journal of Biological Chemistry*, *290*(43), 26314–26327.

McLaughlin, H.M., Sakaguchi, R., Liu, C., Igarashi, T., Pehlivan, D., Chu, K.C., … Antonellis, A. (2010). Compound heterozygosity for loss-of-function lysyl-tRNA synthetase mutations in a patient with peripheral neuropathy. *American Journal of Human Genetics*, *87*(4), 560–566.

Mendes, M.I., Salazar, M.G., Guerrero, K., Thiffault, I., Salomons, G.S., Gauquelin, L, … Bernard, G. (2018). Bi-allelic mutations in *EPRS*, encoding the glutamyl-prolyl-aminoacyl-tRNA synthetase, cause a hypomyelinating leukodystrophy. *American Journal of Human Genetics*, *102*(4), 676–684.

Milligan, J.F., & Uhlenbeck, O.C. (1989). Synthesis of small RNAs using T7 RNA polymerase. *Methods in Enzymology*, *180*, 51-62.

Pakos-Zebrucka, K., Koryga, I., Mnich, K., Ljujic, M., Samali, A., & Gorman, A.M. (2016). The integrated stress response. *EMBO Reports*, *17*(10), 1374–1395.

Park, S.G., Schimmel, P., & Kim, S. (2008). Aminoacyl tRNA synthetases and their connections to disease. *PNAS*, *105*(32), 11043–11049.

Praetorius-Ibba, M., Hausmann, C.D., Paras, M., Rogers, T.E., & Ibba, M. (2007). Functional association between three archaeal aminoacyl-tRNA synthetases. *Journal of Biological Chemistry*, *282*(6), 3680–3687.

Raina, M., Elgamal, S., Santangelo, T.J., & Ibba, M. (2012). Association of a multi-synthetase complex with translating ribosomes in the archaeon Thermococcus kodakarensis. *FEBS Lett*ers, 586(16), 2232–2238.

Robinson, J.C., Kerjan, P., & Mirande, M. (2000). Macromolecular assemblage of aminoacyl-tRNA synthetases: Quantitative analysis of protein-protein interactions and mechanism of complex assembly. *Journal of Molecular Biology*, *304*(5), 983–994.

Rye-McCurdy, T., Rouzina, I., & Musier-Forsyth, K. (2015) Fluorescence anisotropy-based salt-titration approach to characterize protein-nucleic acid interactions. *Methods in Molecular Biology*, *1259*, 385–402.

Smith, D.R., Doucette-Stamm, L.A., Deloughery, C., Lee, H., Dubois, J., Aldredge, T., … Reeve, J.N. (1997). Complete genome sequence of Methanobacterium thermoautotrophicum ΔH: functional analysis and comparative genomics. *Journal of Bacteriology*, *179*(22), 7135–7155.

Sylvers, L.A., Rogers, K.C., Shimizu, M., Ohtsuka, E., & Söll, D. (1993). A 2-thiouridine derivative in $tRNA^{Glu}$ is a positive determinant for aminoacylation by Escherichia coli glutamyl-tRNA synthetase. *Biochemistry*, *32*(15), 3836–3841.

Uter, N.T., Gruic-Sovulj, J., & Perona, J.J. (2005). Amino acid-dependent transfer RNA affinity in a class I aminoacyl-tRNA synthetase, *Journal of Biological Chemistry*, *280*(25), 23966–23977.

Wakasugi, K., Slike, B.M., Hood, J., Ewalt, K.L., Cheresh, D.A., & Schimmel, P. (2002). Induction of angiogenesis by a fragment of human tyrosyl-tRNA synthetase. *Journal of Biological Chemistry*, *277*(23), 20124–20126.

Woese, C.R., Olsen, G.J., Ibba, M., & Söll, D. (2000). Aminoacyl-tRNA synthetases, the genetic code, and the evolutionary process. *Microbiology and Molecular Biology Reviews*, *64*(1), 202–236.

Yang, X., Li, G., Tian, Y., Song, Y., Liang, W., & Zhang, D. (2018). A rice glutamyl-tRNA synthetase modulates early anther cell division and patterning. *Plant Physiology*, *177*(2), 728–744.

Yao, P., & Fox, P.L. (2013). Aminoacyl-tRNA synthetases in medicine and disease. *EMBO Molecular Medicine*, *5*(3), 332–343.

Zhang, C.M., Perona, J.J., Ryu, K., Francklyn, C., & Hou, Y.M. (2006). Distinct kinetic mechanisms of the two classes of aminoacyl-tRNA synthetases. *Journal of Molecular Biology*, *361*(2), 300–311.

Zhong, J., Rao, X., Xu, J.F., Yang, P., & Wang, C.Y. (2012). The role of endoplasmic reticulum stress in autoimmune-mediated beta-cell destruction in type 1 diabetes. *Experimental Diabetes Research*, *2012*, 1–12.